Nitrogen oxides and ozone production in the North Atlantic marine boundary layer

C. Liousse, F. Dulac, H. Cachier, D. Tanré, Thomas P Carsey, Dean D Churchill, Michael L Farmer, Charles J Fischer, Alexander A Pszenny, Victor B Ross, et al.

JOURNAL OF GEOPHYSICAL RESEARCH, VOL. 102, NO. D5, PAGES 5895–5911, MARCH 20, 1997

Remote sensing of carbonaceous aerosol production by African savanna biomass burning

C. Liousse, F. Dulac, and H. Cachier

Centre des Faibles Radioactivités, Centre National de la Recherche Scientifique et Commissariat à l'Energie Atomique, Gif Sur Yvette, France

D. Tanré

Laboratoire d'Optique Atmosphérique, Centre National de la Recherche Scientifique et Université des Sciences et Techniques de Lille, Villeneuve D'Ascq, France

Abstract. We present an estimate of the yearly flux of total and black carbon aerosols emitted by savanna biomass burning in Africa from satellite data and ground-based measurements. Smoke plumes are identified using visible, near-infrared, and thermal infrared derived information. In the savanna region of our study, these structures could either decrease or increase the visible albedo of advanced very high resolution radiometer (AVHRR). It is hypothesized that variations of chemical composition and particulate size distribution may create such differences. The 5S model [*Tanré et al.*, 1990] is used to simulate radiative transfer through smoke plumes and background atmosphere. The overall uncertainty of the derived aerosol optical depth (τ_a) is 75% and mainly due to the choice in particulate composition and size distribution aerosol. Impact of the aerosol mixture (internal versus external mixture) has been also tested. For smoke plumes a typical value of τ_a (at 0.55 μm) is 0.5, and 0.1 for the background atmosphere. Specific extinction cross sections are calculated using Mie theory applied to different representative aerosol models, allowing the retrieval of aerosol columnar concentrations from aerosol optical depth values and integrated aerosol mass loadings in fire plumes. The overall uncertainty on the determination of aerosol load is estimated to be lower than a factor of 5. The atmospheric carbonaceous aerosol flux from savanna burning in Africa was estimated to be 6.5 Tg C yr^{-1}, which compares with that obtained from emission factor on-site measurements (13 ± 5 Tg C yr^{-1}).

Introduction

Recent model computations have suggested that smoke aerosols could have a significant impact on the Earth radiative balance. Owing to their direct optical properties and their capacity to act as cloud condensation particles, these aerosols could create a surface temperature decrease and counteract the greenhouse effect of anthropogenic gases [*Penner et al.*, 1991, 1992] (also J.E. Penner et al., Climate forcing by carbonaceous aerosols, submitted to *Science*, 1997). Such results point out the need for accurate information on smoke emissions, especially from biomass burning, which is still poorly documented.

Biomass burning occurs primarily in the tropics, and 40% on the African continent during savanna fires [*Seiler and Crutzen*, 1980 ; *Levine*, 1990 ; *Andreae*, 1991]. Two field experiments (FOS-DECAFE 91 and SAFARI 92) including various prescribed savanna fires have recently allowed the sampling and study of aerosols emitted by this biomass burning source, with focus on the determination of the aerosol composition, size distribution, optical properties, aging, and emission factors. The published results [*Cachier et al.*, 1991, 1995; *Cachier*, 1995; *Liousse et al.*, 1995] or in preparation for publication (H. Cachier et al., Particulate emissions during savanna fires in Kruger National Park (South Africa), submitted to *Journal of Geophysical Research*, 1996; hereinafter referred to as submitted paper) are in agreement for the aerosol emission factor by burning biomass. Therefore the main problem remaining for the assessment of the global flux of particles resides in the estimate of the annual amount of biomass burnt by the savanna fires. Such an evaluation is based on estimates of standing biomass and fire efficiency in the different ecosystems and on that of burnt surfaces. They rely primarily on satellite observations during the fire season and are at best given with an uncertainty factor of 2 or 3 [*Lacaux et al.*, 1993, 1995].

Satellite observations may offer another opportunity to perform quantitative studies of smoke emissions at different geographic scales. Indeed, different authors have shown that the detection of smoke plumes was possible over surfaces with low albedos such as water [*Chung and Le*, 1984 ; *Porter and Clarke*, 1997], (also, J.N. Porter et al., Deriving aerosol optical depths over the ocean from AVHRR satellite : modeling studies and validations; submitted to *Journal of Geophysical Research*, 1996) or continental forested surfaces [*Ferrare et al.*, 1990; *Malingreau*, 1990; *Setzer and Pereira*, 1991]. Moreover, *Fraser et al.* [1984] and *Kaufman et al.* [1990a,b, 1992] have retrieved the concentration of aerosols and gases in fire plumes over the Amazonian forest from advanced very high resolution radiometer (AVHRR) data. For the first time, a similar approach is presented here for savanna fire plumes. It will be seen that owing to the intermediate values of savanna surface albedos, the fire plume

Paper number 96JD03404.
0148-0227/97/96JD-03404$09.00

detection in AVHRR visible channel images of savanna regions appears to be a complex procedure.

This work was carried out on AVHRR images of western Africa in order to retrieve the mass of carbonaceous aerosols emitted by individual plumes from African savanna fires. Special focus was put on events which had occurred in December 1990 and January 1991, which was the period of the FOS-DECAFE experiment conducted at Lamto, Ivory Coast. During this campaign, various ground-based and airborne measurements were simultaneously undertaken in prescribed savanna fire plumes [*Lacaux et al.*, 1995]. The present study includes four different steps. The first step aims at locating smoke plumes in the AVHRR images and at measuring their effect on the visible AVHRR albedo. Then the aerosol optical depth is retrieved from the albedo values using the Earth atmosphere radiative transfer model 5S [*Tanré et al.*, 1990], which has been adapted to a savanna biomass burning situation. Uncertainties and sensitivities are evaluated and discussed. The third step includes the calculation of the aerosol mass from the aerosol optical depth values. An assessment of the total flux of carbonaceous aerosols emitted by savanna fires in Africa is presented and compared to that obtained from ground-based emission factor data.

2. Detection of Savanna Biomass Burning Plumes Using AVHRR Data

2. 1. The Data Base

Among satellites that can be used to monitor fire development and smoke plumes, the meteorological NOAA series of polar orbiters has been chosen for their capabilities of daily coverage and multispectral coverage with a 1.1-km resolution in five different channels [*Malingreau*, 1990]. The visible channel 1 (0.58-0.68 μm) and near-IR channel 2 (0.725-1.1 μm) may provide information on surface characteristics and smoke loading [*Ferrare et al.*, 1990; *Kaufman et al.*, 1990a,b]. The near-IR channel 3 (3.55-3.93 μm) may be used to detect bright surfaces (or "hot spots") such as fire points, burning scars, and bare soils, but also clouds with small drop size. Ground radiative temperature may be determined from channels 4 and 5 (10.3-11.3 and 11.5-12.5 μm, respectively) where IR terrestrial energy fluxes are maximum. In these channels, clouds may also be easily distinguished.

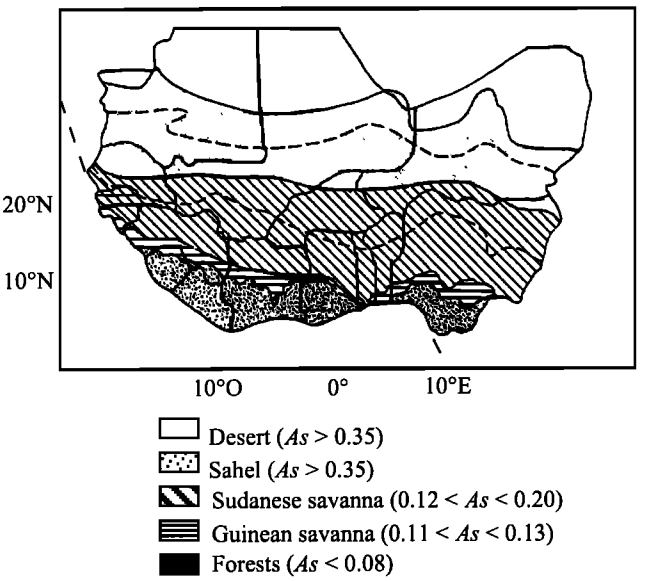

Figure 1. Latitudinal vegetation zones in western Africa with their mean surface albedo (*As*) [from *Bony*, 1975; *Menaut et al.*, 1991; *Arino et al.*, 1992].

A series of six NOAA 11 AVHRR images free of clouds were analyzed in order to observe the western African savannas between 5° and 15°N and 4°E and 16°W. This set consisted of images of 2400 columns by 1600 lines, from the Monitoring of Tropical Vegetation Laboratory, Ispra, Italy. The images were geographically modified using a geographic information system. Their spatial resolution is 1.1 x 1.1 km^2 at nadir. At the edges of the image the resolution may be found to be of the order of 6.5 x 4.5 km^2, which implies an important overlay of pixels. In order to avoid associated errors, the plumes have not been studied in such locations. The area of observation is presented in Figure 1, where the biomass geographic characteristics are also noted. The images selected are from December 5, 6, 7, 13, 14 and 25, 1990, because images realized during the FOS-DECAFE experiment (January 1991) appeared to be unsuitable for the detection of plumes mainly due to the abundance of clouds.

2. 2. Calibration and Uncertainty

Information contained in AVHRR image elements (or pixels) has been converted into physical values with an accurate calibration. For example, the visible AVHRR albedos (A, in percent) have been obtained from digital values (N) of the visible channel 1 as follows :

$$A\,(\%) = 100\,\pi\,w\,\,(\alpha\,N + \beta)\,Ls_{\lambda}^{-1} \qquad (1)$$

where w is the spectral width (0.11 μm^{-1}) relative to channel 1 of the NOAA 11 satellite orbiter, Ls_{λ} is the solar incident radiance at the top of the atmosphere, and α and β, of 0.6 and -24.5, respectively, are the calibration coefficients of channel 1 for the period of our study. Indeed, the variability of these coefficients after the satellite launching has been recently pointed out by *Holben et al.* [1990], *Che and Price* [1992], *Kaufman and Holben* [1993], and *Wu and Zhong* [1994]. Equation (1) can be rewritten as

$$A\,(\%) = \alpha'\,N + \beta' \qquad (2)$$

We determined α' (= 0.114) and β' (= -4.6) using a value of Ls_{λ} of 184.14 W m^{-2}. A corresponds to an albedo for the Sun at zenith.

The uncertainty of the albedo values obviously depends on the accuracy of calibration coefficients and on digital counts:

$$dA/A = d\alpha'/\alpha' + d\beta'/\beta' + dN/N$$

The uncertainty on β' may be neglected, whereas that on α' is of the order of ±7% [*SATMOS*, 1991; *Kaufman and Holben*, 1993]. N absolute uncertainty (dN) was considered to be ±1, whereas the mean value of N currently measured in smoke pixels was 120. Therefore the albedo total relative error dA/A is of the order of ±8%.

2. 3. Theoretical Aerosol Impact on the Visible Radiance

Figure 2 presents the visible atmospheric albedo (ΔA), which is the difference between the apparent visible albedo measured by the satellite sensor (A) and the surface albedo (As), as a function of the surface albedo for various aerosol optical properties. First, we may note that the impact on ΔA of an aerosol layer depends

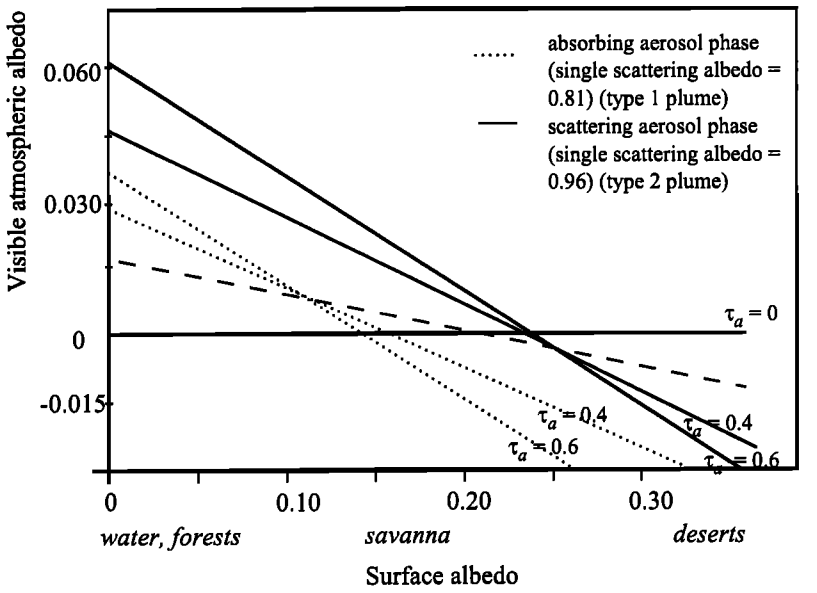

Figure 2. Change in visible atmospheric albedo as a function of surface albedo for different values of the aerosol optical depths for aerosol models with two different single scattering albedo. Dotted and solid lines correspond to absorbing and scattering aerosol model impact, respectively. The dashed line represents Rayleigh scattering influence [from *King et al.*, 1992].

on *As*. Over a dark surface (*As* < 0.1), the backscattering of the incident radiation in the atmosphere dominates, so that *A* is larger than the surface albedo whatever the aerosol type: ΔA is systematically positive in the presence of an aerosol layer. On the other hand, over a bright surface (*As* > 0.3) the aerosol absorption and backscattering of the radiation reflected by the surface dominate, so that *A* is lower than the surface albedo and ΔA is negative. Over surfaces with intermediate values of *As* the radiative effect may be undetectable. The surface albedo value for which an aerosol layer has no effect on the visible atmospheric albedo is called the critical surface albedo. For surface albedos close to this value, a given aerosol layer may have slight but opposite effects. The critical surface albedo is strongly dependent on the aerosol single scattering albedo and, to a lesser extent, on particle size [*Fraser and Kaufman*, 1985; *Kaufman*, 1987; *King et al.*, 1992]. So, following the previous theoretical considerations, it appears that aerosol remote sensing will be of variable difficulty.

The surface albedo values of savanna soils for the region of our study, given in Figure 1, are included in the range of the critical surface albedo values. So, over a given savanna site with a surface albedo value of 0.16, for example, smoke plumes are expected to be detected with different effects, depending on their single scattering albedo: some increasing the visible atmospheric albedo and others decreasing it.

2. 4. Methods

A protocol was developped in order to identify savanna fire plumes on the images. Various software [*Sutton et al.*, 1988; *Vogt*, 1990] (Sphinx®; Imassist®) were used in order to perform graphics and digital calculations such as image display, window extraction, zooming, thresholding, and false color composition.

As biomass burning smoke plumes must include fire pixels, the first step of our method was to map the active fires. Our images have been thresholded in accordance with previous studies [*Kaufman et al.*, 1990a; *Brustet et al.*, 1991 ; *Grégoire et al.*, 1993] which have shown that the use of different IR channels is needed to separate the impact of the fire pixels from that of the bare soils and burning scars. Briefly, the fire pixels have been discriminated from other pixels using the following rules determined by *Franca et al.* [1995] for the African savanna:

Channel 3 temperature > 320 K (fire pixels must saturate channel 3).

Channel 4 temperature > 287 K (this test allows us to discriminate fires from strong reflective clouds which may also sature channel 3.)

Channel 3 temperature - channel 4 temperature > 15 K (this test is used to separate fires from hot surfaces).

0 < channel 4 temperature - channel 5 temperature < 5 K (this test is especially used to determine fires from partial clouds).

A (visible AVHRR albedo) < 9.5 % (this test allows us to confirm presence of active fire pixels which are used to affect visible albedo).

By comparing these fire pixel maps and the original images visualized in grey levels, we identified in cloud-free regions many elongated structures originating from fire plots and occurring in the dominant northeasterly wind direction. We used a false color composition in order to obtain further evidence of the presence of smoke plumes in these structures. This technique consists of assigning one of the three basic colors (red, blue, green) to one of the three different channels (visible, near infrared, and infrared), which are then combined to display a color composite image [*Chung and Le*, 1984; *Malingreau et al.*, 1989]. The IR channel was red, the near-IR channel green, and the visible blue. This is the most convenient composition to determine vegetation changes and aerosol impact [*Malingreau et al.*, 1989]. In such a composition, areas with wet or dry vegetation appear in green or yellow, respectively, water and lake in claret or deep purple, clouds in blue, and burning scars or bare soils in red or pink. In the following, we shall see that two types

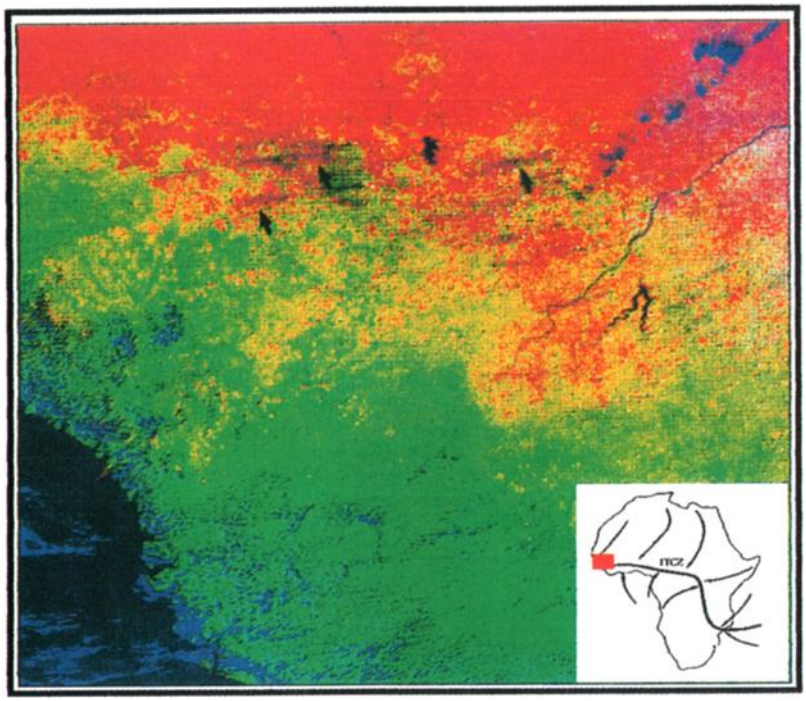

Plate 1. False color composite image (from NOAA AVHRR data for December 5, 1990).

of smoke plumes are detected in such a composition, with either a brownish or a purple color.

Once the smoke plumes are identified, a more quantitative approach is performed. On a single image with no cloud events, we considered two types of pixels : pixels within the smoke plume events and pixels situated in the vicinity of smoke pixels (called background pixels). Background pixels were assumed to never be directly affected by smoke events, but they may be highly polluted by the presence of the aged biomass burning aerosols resulting from previous fires. For example, the site of Lamto (with experimental optical depths of the order of 1 during the fire season [*Liousse et al.*, 1995]) may be representative of a situation of background atmosphere. Of course, the boarders between the two kinds of pixels are fictive, as the plumes really fade into a more or less polluted background. Smoke pixels may be distinguished when the difference between their visible AVHRR albedo and that of the background are at least larger than the relative error on the AVHRR albedo. With the use of this method, we assumed that background atmosphere under the plumes was the same as that surrounding the plumes. This hypothesis was tested and validated with the method set up by *Kaufman et al.* [1990a,b] using an additional image. Indeed, the same location was studied with two different cloudless images, one (the December 6 image) when the site was covered by a smoke plume, the other (the December 5 image) when the site has no smoke events, which corresponds to a situation of background atmosphere. The mean albedo value (of 11%) measured in the background within a 10-km area all around a given plume with our simple method using the December 6 image was equal to the mean visible AVHRR albedo measured with the method of Kaufman et al. in the December 5 image. Moreover, the use of a single image for determining the albedo of the background removes the additional uncertainty due to the change in the geometry of observation if different images are used.

2. 5. Results

Plate 1 shows an AVHRR image taken on December 5, 1990. The savanna areas mainly appear cloud less: this situation is confirmed by a meteorological survey (*J.M. Grégoire*, personal communication, 1995). The fire spatial distribution is superimposed on the image, and fire pixels may be discriminated by their white color. At this period, fires are found distributed over the whole Sudanese savanna area (9°-14°N). A careful look at the successive images has shown that the fire development occurred from east to west, a phenomenon which is in agreement with previous field observations of local fire ignition [*Monnier*, 1968]. Some fires may also be noticed in the Guinean savanna region, where the dry season is not yet established. Some brownish smoke plumes appear parallel to the wind direction. In fact, about 90% of the detected smoke plumes, called type 1 plumes, were made up of brownish smoke plumes. The other 10% of the plumes, called type 2 plumes, mainly appear in light purple, but they do not appear in Plate 1.

Table 1a shows the visible AVHRR albedo values obtained for one of the detected type 1 smoke plumes: following the rules described in section 2.4, it may be seen that smoke plume and background pixels are distinguished. In that case, mean albedo values are (8.5±0.3)% and (11.0±0.3)%, respectively. Inside the type 1 smoke plume structure, values are not constant and pixels may be classified in two quasi-uniform parts, in which absolute variations in the AVHRR albedo are within 1% with increasing distance from the origin of the plume. The first part of the plume, close to the source, is highly contaminated by smoke. The properties of the second part are close to that of the background. Same observations were performed for the type 2 smoke plume structure (Table 1b). Near the active fire pixels, due to the presence of aerosol, the albedo also decreases relative to the background. However, differences between type 1 and type 2

Table 1a. Example of Visible AVHRR Albedo Values for a Type 1 Plume of the West Zone (see Tables 3 and 5)

Geographic Pixel Position (Line n°)											
28	29	30	31	32	33	34	35	36	37	38	39
10.4	10.4	10.4	10.4	9.1[a]	8.5[a]	8.5[a]	7.9[a,b]	7 9[a,b]	10 4	11.0	11.0
10 8	10.4	10.4	10.4	8.5[a]	8 5[a]	7.9[a,b]	7.9[a,b]	7 9[a,b]	10.4	10.4	11.0
10.8	10.4	10.4	9.1[a]	8.5[a]	8 5[a]	7.9[a,b]	8.5[a]	8.5[a]	10.4	10 4	11.0
10.4	10.4	10.4	9 1[a]	8.5[a]	8.5[a]	8.5[a]	8.5[a]	8.5[a]	10 8	10.8	11.0
9.1[a]	9.1[a]	9 1[a]	9.1[a]	8.5[a]	8.5[a]	8.5[a]	8 5[a]	10.4	10 4	11.0	11 0
10.4	9.1[a]	9.1[a]	8 5[a]	8.5[a]	8.5[a]	10.4	10.4	10.8	10 8	11.0	11.0
10.4	10.4	9.1[a]	9.1[a]	9.1[a]	9.1[a]	10 4	10.4	11.0	11 0	11.0	11.0
10 8	10.8	10.4	10.4	10.4	10.4	10 4	10.8	11 0	11.0	11.0	11.0
10.8	10.8	10.8	10.8	10.4	10.4	10.4	10.8	10 8	11 0	11.0	11.0
11.0	10.8	11.0	11.0	11.0	11.0	10.8	10.8	10 8	11.0	11.0	11.0

Values are in percent and are background atmosphere pixels unless otherwise noted
[a] Smoke plume pixels.
[b] Burnt area of plume event.

plumes appear in the other part of the structure, where the visible AVHRR albedo can be either decreased (type 1) or increased (type 2) by smoke particles.

In our study for each type of plume, we considered a mean AVHRR albedo. Values are presented in Table 2 for the southeastern areas described in Figure 1.

In cases presented in Table 1, the overall length of a smoke plume is of the order of 10 km. In our whole study, smoke plume lengths have been included in the 5 to 30-km range. Longer smoke plumes (up to 50 km) have been found over the southeastern Sudanese savannas, but the presence of fire pixels in the center of the plumes suggested that these longer smoke plumes combined at least two or three smaller ones.

It is interesting to understand now why type 1 and type 2 plumes are brownish and purple structures, respectively. As previously described, type 1 plumes decrease visible atmospheric albedo values (or pixel values from the blue channel), whereas type 2 structures increase these values. Also, the apparent

Table 1b. Same as Table 1a but for a type 2 Plume

57	58	59	60	61	62	63	64	65	66	67	68
10.3	10.3	10.3	10.3	10.3	10 3	10.3	10.3	10.3	9.3[a,b]	9.3[a,b]	10.3
10.3	10.3	10.3	10.3	10.3	10.3	10.3	10.3	10.3	9.3[a,b]	9 3[a,b]	9.3[a,b]
10.3	10.3	10.3	10.3	10.3	10.3	10.3	10.3	12.2[a]	12.2[a]	9.3[a,b]	9.3[a,b]
10.3	10.3	10.3	10.3	10.3	12.2[a]	12.2[a]	12.2[a]	13[a]	13[a]	9.3[a,b]	9.3[a,b]
10.3	10 3	10.3	10.3	12.2[a]	12.2[a]	13[a]	13[a]	13[a]	12.2[a]	9.3[a,b]	9.3[a,b]
10.3	10.3	10.3	10.3	12.2[a]	12.2[a]	13[a]	13[a]	13[a]	12.2[a]	10.3	10.3
10.3	10.3	12.2[a]	12.2[a]	12.2[a]	13[a]	13[a]	13[a]	13[a]	12.2[a]	12.2[a]	10.3
10.3	12.2[a]	12.2[a]	12.2[a]	13[a]	13[a]	13[a]	13[a]	13[a]	13[a]	12.2[a]	10.3
12.2[a]	12 2[a]	12.2[a]	12.2[a]	12.2[a]	13[a]	13[a]	13[a]	13[a]	13[a]	13[a]	12.2[a]
12.2[a]	12.2[a]	12.2[a]	12.2[a]	12.2[a]	13[a]	13[a]	12.2[a]	12.2[a]	12.2[a]	12.2[a]	12.2[a]
12 2[a]	12.2[a]	12.2[a]	12.2[a]	12.2[a]	12.2[a]	12.2[a]	12.2[a]	12.2[a]	12.2[a]	12.2[a]	12.2[a]
12.2[a]	12.2[a]	12.2[a]	12.2[a]	10.3	10.3	10.3	10.3	10.3	10.3	10.3	10.3
12.2[a]	10.3	10.3	10.3	10.3	10.3	10.3	10.3	10.3	10.3	10.3	10.3

Values are in percent and are background atmosphere pixels unless otherwise noted.
[a] Smoke plume pixels.
[b] Burnt area of plume event.

Table 2. Average Values for Eastern Area of Visible AVHRR Albedos, Aerosol Optical Thickness, and Relevant Average Aerosol Mass Loadings in Smoke Plumes, and in Background Atmosphere

	Background	Type 1 Plume	Type 2 Plume
Visible AVHRR Albedo, %	11	8	12.6
Aerosol Optical Thickness	0.1	0.45	0.5
Specific Extinction Cross Section, $m^2 g^{-1}$	1.35	1 7	4.6
Aerosol Mass Load, $g m^{-2}$	0.07	0.265	0 11

temperature calculated from the red IR channel is higher in type 1 plumes than in the background, whereas it is lower in type 2 plumes (ΔT is of the order of 1 to 10°K). Let us note that, as both type 2 plumes and clouds decrease the apparent temperature, they needed to be discriminated. This was achieved by reporting the IR temperature and the visible albedo of purple plumes in the Lijlas diagram [*Lijlas*, 1987; *Franca et al.*, 1995].

Among all the possible explanations, we may present the following hypothesis.

For a constant savanna surface albedo, according to Figure 2, brownish plumes which decrease the mean AVHRR albedo should be loaded by absorbing particles with a single scattering albedo (ω_o) lower than 0.8, whereas purple plumes should have particles with less absorbing capabilities and a single scattering albedo higher than 0.9. The ω_o variability may also result from the variability of aerosol size and/or composition. Apparent temperature, which has been seen to be higher in the brownish plumes and lower in the purple plumes than in the background atmosphere, may reveal the height of the aerosol layer. Apparent temperature combines both the surface and the atmospheric temperature. As shown by *Robock* [1991], illumination near the ground is usually reduced by smoke particles, which leads to lower IR emissions and, consequently, lower surface temperature. It may be assumed that this situation occurs for both kinds of plumes. Therefore the differences in temperature between type 1 and 2 plumes could originate from the plume temperature itself, particles found in type 1 plumes having higher temperature than those in type 2 plumes. This may be due to the vertical location of the particles: the brownish type 1 plumes would be confined in the lower atmospheric layers owing to low vertical buoyancy, whereas type 2 plumes would have an important vertical development and would be thus situated in higher atmospheric layers. As a consequence, aerosols in type 2 plumes would be older and then bigger than those in type 1 plumes. According to the theoretical curves given by *Twomey* [1977], we may deduce that the larger the particles, the larger the scattering effect, and the higher the single scattering albedo values. Moreover, savannas may burn under different flaming conditions, heading or backing fires, the most violent fires (the heading fires) having a larger buoyancy and producing aerosols with lower black carbon contents (H. Cachier et al., submitted paper, 1996]. These two types of savanna burning lead to different types of plumes.

2. 6. Discussion

The spatial distribution of visible AVHRR albedo of plumes was studied over western African savannas. Smoke plumes were

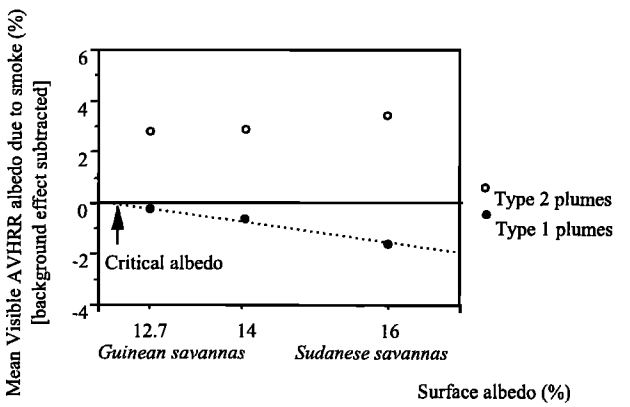

Figure 3. Visible AVHRR albedo relative to smoke in % as a function of surface albedo in % (background effect subtracted).

detected in three main savanna ecosystems presented in Figure 1. The relevant surface albedo values have been obtained from *Bony* [1975] and *Arino et al.* [1992] : 16% for the Sudanese savanna, 13% for the Guinean savanna, and 14% for a mixture of the two previous ecosystems (grassland with a 10% wood tree cover). These values, which are representative of actual surface reflectance values, cannot be directly compared to apparent background albedos obtained in this work, since our values are not corrected for the background atmospheric pollution. Figure 3 presents the increment of visible AVHRR albedo measured in either type 1 and type 2 plumes as a function of the surface albedo for the three considered ecosystems. In agreement with the theoretical computation (Figure 2), the effect of type 1 plumes appears to be dependent on the surface albedo and, consequently, on the vegetation cover. The larger the surface albedo, the more important the effect and the easier the type 1 plume observation. Indeed, whereas remote sensing of plumes seems to be easy above the dry Sudanese savanna (surface albedo of 16%), in the Guinean humid savanna with lower surface albedo (13%), some smoke structures are likely to be undetectable. However, there is no linear relationship between surface albedo and visible AVHRR albedo for type 2 plumes: it seems that they are easily observed whatever the type of savanna. According to Figure 2, the detection of type 2 plumes should have been more difficult over the Sudanese savannas of higher surface albedo. This absence of difference might be due to the variability of smoke particle properties previously described within these plumes.

3. Retrieval of the Aerosol Optical Depths

An Earth uncloudy atmosphere radiative model derived from the computer code "5S" ("Simulation of the Satellite Signal in the Solar Spectrum") [*Tanré et al.*, 1990] was used to retrieve the aerosol optical depth from visible AVHRR albedo values. Our period of observation being situated before the Pinatubo event, stratospheric aerosol optical depth values [*McCormick and Veiga*, 1992] could be neglected. A particular effort was conducted with the aerosol phase model in relation to our ground-based measurements.

3. 1. Description of the Method Principle

The 5S code allows the simulation of the satellite signal due the reflection of the light by the ground-atmosphere system in the solar spectrum (0.35-4 μm), assuming a cloudless atmosphere.

Table 3. Geometric Conditions of West Africa Remote Sensing and Surface Albedo Values

Zone	Latitude	Longitude	Image Date	Savanna Type	Surface Albedo	Observation Hours	Pixel Number on Image Line	Ascendant node Time	Ascendant node Longitude	θ_s	θ_v	ϕ_s	ϕ_v
Middle	9°	-7°	Jan. 11, 1991	Guinean	0.127	14.63245	1038	14.58905	355.9818	43°28'	0°52'	224°37'	80°52'
West	13°27'	-13°48'	Dec. 7, 1990	Sudanese	0.16	14.4445	1885	14.3725	358.64	43°26', 48°55'	0°52', 55°23'	214°44', 224°16'	78°28', -99°14'
East	10°4'	-2°34'	Dec. 5, 1990	Sudanese	0.16	14.79126	300	14.7478	352.98	49°47', 52°2'	28°44', 45°41'	229°12', 231°27'	-98°31', -98°2'

Here, θ_s, zenith solar angle; θ_v, azimuthal solar angle; ϕ_s zenith observation angle; ϕ_v, azimuthal angle.

An exhaustive description of the calculations performed by 5S may be found by *Tanré et al.* [1990]. Briefly, this code is based on a detailed description of spectral scattering by the surface, atmospheric gases, and aerosols. A correction is made to account for the absorption of the atmospheric gases H_2O, O_3, O_2, and CO_2. The particulate multiple scattering is approximated. An approximation for the multiple interactions between gases and aerosols is also performed. The error consequent upon this approximation has been shown to be of the order of a few percent [*Tanré et al.*, 1992].

The aerosol optical depth at 550 nm (τ_a) is the parameter used to set the aerosol concentration. Following the method used by *Dulac et al.* [1992] for the study of desert dust plumes, the code is used to simulate the visible AVHRR albedo for a number of values of τ_a, depending on the input parameters of the 5S model, such as the geometric and spectral conditions, the surface albedo, the atmospheric gaseous composition, and the aerosol type and concentration. Such simulations were performed for smoke contaminated pixels and for pixels with background atmosphere.

Table 3 summarizes the geometric and the surface albedo input parameters needed to simulate satellite observations in the three typical areas of western African savannas where smoke plumes have been detected. Following experimental results [*Fishman et al.*, 1990; *Liousse et al.*, 1995], larger atmospheric H_2O and O_3 contents (6 g cm^{-2} and 0.344 cm atm, respectively) were considered for the simulation of smoke plumes than for the background atmosphere (4 g cm^{-2} and 0.247 cm atm). Profiles of pressure and temperature from either the US62 model or the 5S tropical atmosphere model [*McClatchey et al.*, 1971] yielded similar results. Our parallel ground-based results show that savanna biomass burning aerosols combine four basic particle components [*Cachier et al.*, 1995]: organic carbon (OC), black carbon (BC), submicron-size water-soluble particles (WS), and mineral dust particles (D). Because the basic standard aerosol components defined in the work by the World Meteorological Organization (WMO) [1986] and used by the 5S code did not allow us to simulate organic carbon particles, which are known to be the major fraction of biomass burning aerosols [*Cachier et al.*, 1991 ; *Mazurek et al.*, 1991], a new aerosol model has been defined. Also, in order to take into account the aerosol size distribution variability linked to various smoke ages, we developed aerosol models with different particle sizes. Table 4a presents the different characteristics used to compute particle relevant optical properties. Absorption and scattering spectral properties of all these aerosol models were computed using Mie theory [*Van de Hulst*, 1957], which assumes homogeneous spherical particles. Because parameters relative to the organic carbon particle model are not supported by many data, further calculations will be needed when new experimental measurements are available.

Furthermore, recent experiments have shown that combustion particles are generally internally mixed [*Parungo et al.*, 1992; *Herring et al.*, 1995; *Hobbs et al.*, 1997; *Echalar*, 1995]. Then, following these references and calculations by *Ackerman and Toon* [1981] and *Sloane* [1983, 1984], we performed simulations of heterogeneous particles, considering they consisted of a homogeneous core coated with a uniform shell. The core particle size was taken in the upper part of the accumulation mode for BC, OC, and WS particles and in the coarse mode for dust. We tested shells representing 1% or 10% of the total particle volume. These models are listed in Table 4b.

3. 2. Results

Aerosols in the background atmosphere and in type 1 and type 2 plumes were simulated separately. Chemical composition and particle size for the three different conditions were chosen in accordance with ground-based measurements and are reported in Table 5a.

Type 1 and type 2 plumes are mainly composed of organic carbon particles. Following previous field measurements [*Cachier et al.*, 1995], we have differentiated the BC/OC ratio in particles. Black carbon relative content was assumed to be higher in background than in plumes.

Table 4a. Aerosol Models for External Mixtures

Model	Symbol	ri, μm	σ_g	m	ρ, g/cm^3	Reference
Black Carbon	BC(0.015)	0.006	1.7	1.95-0.66i	1-2	*Bergström* [1972]; *Whitby* [1978]
	BC(0.04)	0.015	1.7	1.95-0.66i	1-2	*Bergström* [1972]; *Whitby* [1978]
	BC(0.05)	0.0118	2	1.75-0.45i	2.3	*WMO* [1986]; *D'Almeida et al.* [1991]
	BC(0.1)	0.04	1.7	1.95-0.66i	1-2	*Bergström* [1972]; *Whitby* [1978]
	BC(0 15)	0.065	1.7	1.95-0.66i	1-2	*Bergström* [1972]; *Whitby* [1978]
	BC(0.8)	0.2	2	1.95-0.66i	1-2	*Bergström* [1972], *Whitby* [1978]
Organic carbon	OC(0.01)	0.002	1.7	1.43-0 0035i	1.7-2	*Holben et al.* [1991]; *Sloane* [1983]
	OC(0.015)	0.006	1.7	1.43-0.0035i	1.7-2	
	OC(0.03)	0.015	1.7	1.43-0.0035i	1.7-2	
	OC(0.1)	0.04	1.7	1.43-0.0035i	1.7-2	*Holben et al.* [1991]; *Sloane* [1983]
	OC(0.15)	0.065	1.7	1.43-0.0035i	1.7-2	
	OC(0.2)	0.086	1.7	1.43-0.0035i	1.7-2	
	OC(0.45)	0.2	1.7	1.43-0.0035i	1.7-2	*Holben et al.* [1991]; *Sloane* [1983]
	OC(0.8)	0.2	2	1.43-0.0035i	1.7-2	
Water soluble	WS(0.18)	0.005	2.99	1.53-0.005i	1.7-2	*WMO* [1986]; *D'Almeida et al.* [1991]
	WS(0.8)	0.2	2	1 53-10^{-7}i	1.7-2	*Whitby* [1978]
Dust-like	D(18)	0.5	2.99	1.53-0.008i	1.6-2.7	*WMO* [1986]; *D'Almeida et al.* [1991]
	D(12.2)	2.3	2.11	1.5-0.0008i	2-2.3	*Ackerman and Toon* [1981]; *Patterson and Gillette* [1977]

Volume mean radius is into parentheses; r_l, mean geometric radius ; σ_g, geometric standard deviation; m, complex refractive index; ρ density.

Table 4b. Aerosol Models for Internal Mixtures

Model	Symbol	r_i, μm	σ_g	m	ρ, g/cm^3	Reference
Organic carbon shell and black carbon core	BC/OC [a]		1.7	1.43-0.0035i	1.7-2	*Holben et al.* [1991], *Sloane* [1983]
				1.95-1.66i	1-2	*Bergström* [1972]; *Whitby* [1978]
Water-soluble shell and black carbon core	BC/WS [a]		1.7	1.53-10^{-7}i	1.7-2	*Whitby* [1978]
				1.95-1.66i	1-2	*Bergström* [1972]; *Whitby* [1978]
Water shell and black carbon core	BC/water [a]		1.7	1.33	2	*Whitby* [1978]
				1.95-1.66i	1-2	*Bergström* [1972], *Whitby* [1978]
Water shell and organic carbon	OC/water [a]		1.7	1.33	2	*Whitby* [1978]
				1.43-0.0035i	1.7-2	*Holben et al.* [1991], *Sloane* [1983]
Water shell and dust core	D/water [b]		2.11	1.33	2	*Whitby* [1978]
				1 50-0.0008i	2.3	*Ackerman and Toon* [1981]; *Patterson and Gillette* [1977]
Organic carbon shell and dust cores	D/OC [b]		2.11	1.43-0 0035i	1 7-2	*Holben et al* [1991]; *Sloane* [1983]
				1.50-0.0008i	2.3	*Ackerman and Toon* [1981], *Patterson and Gillette* [1977]
Organic carbon shell and water-soluble core	WS/OC [a]		1.7	1.43-0.0035i	1.7-2	*Holben et al.* [1991]; *Sloane* [1983]
				1.53-10^{-7}i	1.7-2	*Whitby* [1978]
Water shell and water-soluble core	WS/water [a]		1.7	1.33	2	*Whitby* [1978]
				1.53-10^{-7}i	1.7-2	*Whitby* [1978]

Here, r_i, mean geometric radius; σ_g, geometric standard deviation; m, complex refractive index; ρ, density
[a] 1% mix: internal r_i, 0.198 μm, external r_i, 0.2 μm; 10% mix: internal r_i, 0.192 μm, external r_i, 0.2 μm.
[b] 1% mix: internal r_i, 2.29 μm, external r_i, 2.3 μm; 10% mix: internal r_i, 2.22 μm, external r_i, 2.3 μm.

A literature data survey points out an important variability of the volume mean radius of biomass burning particles in the range 0.015 μm to 1.0 μm (see Table 5b). Among other determinants, aging of particles is certainly an important parameter. This aging is accompanied by formation of coatings onto particles coming from liquid condensation of water and/or adsorption and conversion of various gaseous substances. Coagulation and sintering processes [*Richmond and Flagan*, 1994] occurring during particulate aging could also change black carbon aggregates into larger particles.

Thus, according to these literature data, we present our best guess for aerosol size distribution in the three clearly different situations: type 1 and type 2 plumes and background conditions (Table 5a). Since type 1 plumes have been considered as young plumes (section 2.5), it is assumed that they are mainly composed of young and small particles with a volume mean radius for organic carbon particles of 0.03 μm. In contrast, type 2 plumes have been hypothesized to develop in altitude and to contain older and larger particles: mean volume radius for the main component (the organic carbon particles) was assumed to be 0.1 μm. That of black carbon and sulfates has been chosen in the largest part of the possible range (Table 5b). Moreover, these particles were considered to be mainly internally mixed. Finally, in the background atmosphere, we considered that the aerosol phase was dominated by dust particles with volume mean radius larger than in plumes.

Based on the 5S model, relationships between visible AVHRR albedo and aerosol optical depth have been established for background and type 1 and type 2 plumes. Figure 4 shows such relationships for plumes detected over eastern areas. From these curves, visible AVHRR albedo values could be converted into aerosol optical depths at 550 nm. Optical depths due to the plume smoke only, were obtained by subtracting the background

Table 5a. Aerosol Models Used for the Retrieval of τ_a in Type 1 and Type 2 Plumes and in Background Atmosphere

	Percent
Background atmosphere	
$OC^{(0.03)}$	30 4
$BC^{(0.04)}$	7.6
$D^{(18)}$	50.0
$WS^{(0\ 8)}$	12 0
Brownish plume	
$OC^{(0\ 03)}$	81.4
$BC^{(0.04)}$	12.0
$D^{(12.2)}$	4.9
$WS^{(0.18)}$	1.7
Purple plume	
$OC^{(0\ 1)}$	87.0
$BC^{(0.8)}/OC^a$	11.0
$D^{(12.2)}/OC^a$	0.5
$WS^{(0.8)}/OC^a$	1.5

[a]Coating of organic carbon.
Volume mean radius chosen for each particle is indicated in parentheses. More details are given in Tables 4a and 4b.

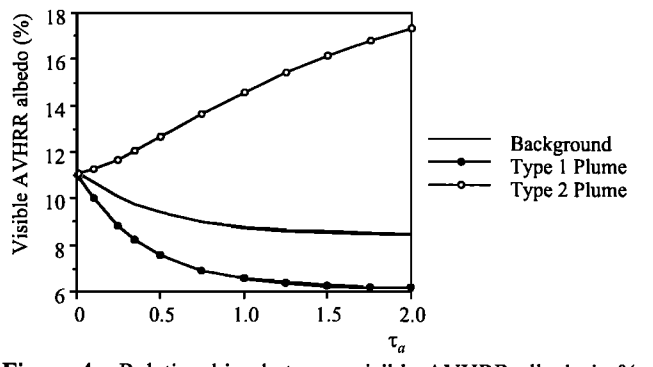

Figure 4. Relationships between visible AVHRR albedo in % and aerosol optical depth obtained by 5S model for type 1 and type 2 plumes, and background atmosphere of the eastern area. Parameters are described in Tables 3 and 5.

Table 5b. Aerosol Volume Distributions Given in the Literature for Smoke Particles

	r_v	σ_g	Reference
		Theoretical Calculations	
Black Carbon	0.04-0.1	2	*Chylek et al.* [1981]
Black Carbon	0 015	1.7	*Bergström et al.* [1982]
Black Carbon	0.015-0.2	1.7	*Ackerman and Toon* [1981]
Black Carbon	0.015-0.8	1.7	*Whitby* [1978]
		Experimental Data	
Haze Layers, Amazonia			
Smoke	0.12	1.7	*Andreae et al.* [1988]
Tropical South Atlantic			
Smoke	0.1	1.7	*Andreae et al.* [1994]
Haze Layers, South Africa			
Smoke	0.1	1.7	*Le Canut et al* [1996]
Background particles	0.2	1.7	
Amazonia			
Smoke	0 25	2	*Kaufman and Holben* [1993]; *Kaufman et al.* [1994]
Background particles	0.7	2	*Kaufman and Holben* [1993]; *Kaufman et al* [1994]
Northern America			
Fires	0.12	1.7	*Radke et al.* [1988]
Background particles	0.22	1.7	*Radke et al.* [1988]
Savanna Fires			
Smoke	0.3	1.7	*Liousse et al.* [1995]
Background particles	1.21	1.7	*Liousse et al.* [1995]

r_v, mean volume radius, μm; σ_g, geometric standard deviation.

contribution. For a «mean situation», as presented in Table 2, the τ_a background value is of the order of 0.1. This value is in the lowest part of the range of aerosol optical depth experimentally measured in the Ivorian savanna during the FOS-DECAFE experiments in the 1991 fire season [*Liousse et al.*, 1995]. In type 1 and type 2 plumes the average smoke contributions to τ_a are of the order of 0.5. No typical difference may be found between the two kinds of plumes. The variability in τ_a within the three zones (selected in Table 3) is found to be of the order of 25%.

3. 3. Uncertainties

Sensitivity tests were performed in order to evaluate the absolute uncertainty in the retrieval of aerosol optical depths. In view of such evaluations, a given parameter among the viewing geometry, surface albedo, atmospheric gaseous concentrations and aerosol size, and chemical composition was allowed to vary in a realistic range for the atmospheric conditions of our study. Uncertainty was then determined for a fixed albedo value corresponding to our average measurements.

3. 3. 1. Tests on viewing geometry, surface albedo and gaseous concentrations. We considered the same mean geometry inside each of the three selected zones. However, the change in the Sun and viewing angles may be significant inside a given zone. For example, in the east zone, the observations realized over the northern half may be characterized by θ_s = 49.79°, θ_v = 28.73°, ϕ_s = 229.20°, and ϕ_v = -98.52°, and those of the southern half by θ_s = 52.03°, θ_v = 45.69°, ϕ_s = 231.45°, and ϕ_v = -98.03°. Running the 5S model for these two geometrical conditions, the other parameters being constant, we found that the uncertainty on the retrieved aerosol optical depth values is of the order of 10%. Such a variation has also been observed in the western zone. This variation is mainly due to the anisotropy of the backscattering aerosol properties. Recent works [*Gutman et al.*, 1989; *Roujean et al.*, 1992] have shown that anisotropy of the surface reflectance might also occur, which will require further investigations.

Testing the impact of surface albedo variability in the retrieval of τ_a, we could evaluate that a surface albedo uncertainty of 10% results in an uncertainty of 5-20% for τ_a values, the smaller uncertainty being associated to higher aerosol concentrations. For a mean AVHRR albedo corresponding to an aerosol optical depth of 0.5, uncertainty on τ_a values is of the order of 10%.

Finally, impact of changes in H_2O and O_3 atmospheric contents was investigated. For this purpose, we took extreme values experimentally obtained in background (4 g/m^2 and 0.247 cm atm) and in plume conditions (6 g/m^2 and 0.344 cm atm). Tests showed that for a given visible AVHRR albedo, maximum error on τ_a retrieval was then less than 10%.

3. 3. 2. Tests on aerosol models. The optical properties of the aerosol phase and, consequently, their impact on the assessment of τ_a are governed by several factors.

First, the scattering capability of the aerosol phase depends on the real part of its refractive index and the absorption capability on its imaginary part.

Second, the particle size distribution also influences aerosol optical properties, as shown by theoretical studies on scattering and absorbing cross sections, the single scattering albedo, and the backscattering parameters [e.g., *Fenn and Oser*, 1965].

Third, considering external or internal mixing for the aerosol phase also changes the aerosol optical properties. Heterogeneous particles generally found in the accumulation mode are larger than homogeneous particles. This has been illustrated by *D'Almeida et al.* [1991], who calculated the growth of black carbon particles with the atmospheric relative humidity (RH) and found that the particle radii may double with RH ranging from 0 to 99%. Also, the presence of a shell at the surface of an

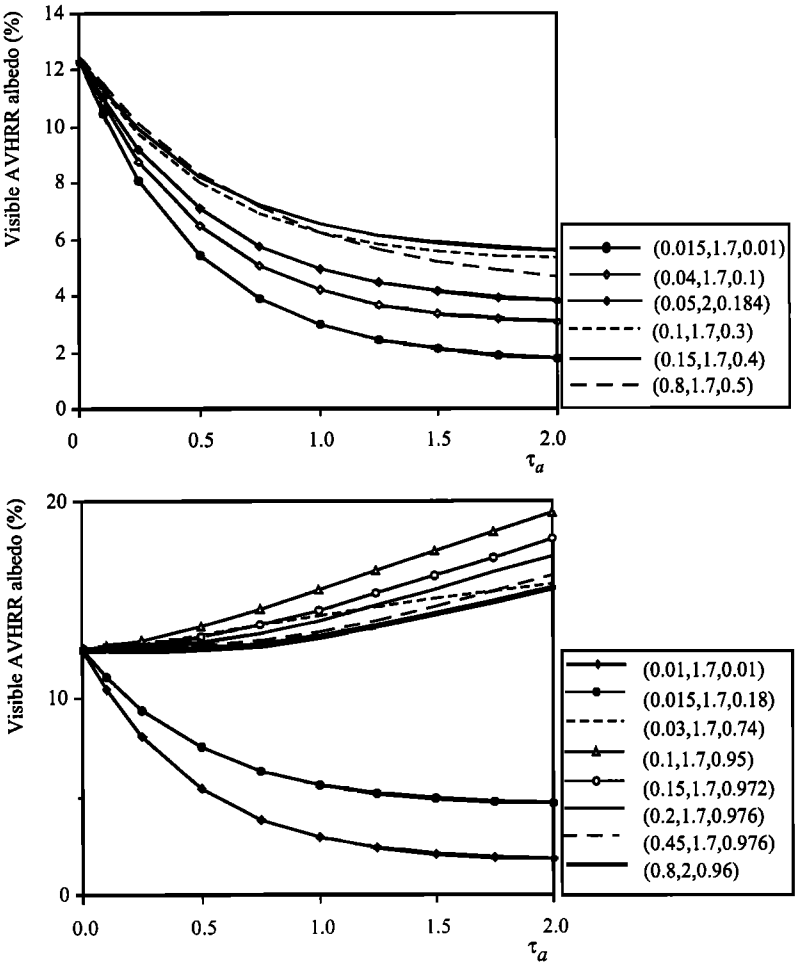

Figure 5. Impact of particle size on the relationship between visible AVHRR albedo in % and aerosol optical depth (τ_a) (volume mean radius, geometric deviation, and single scattering albedo values (or ω_o) are indicated into parentheses). Tests for a smoke plume atmosphere (see Table 5a) with a single component aerosol type. (top) Black carbon studies. (bottom) Organic carbon studies.

absorbing core such as black carbon particles may focus the incident radiation toward the inner part of the core, as the surface material real refractive index is lower than that of the black carbon core. In such a situation, the core absorptive capacity is significantly reinforced [*Fenn and Oser*, 1965; *Ackerman and Toon*, 1981; *Bergstrom et al.*, 1982; *Rosen and Novakov*, 1984; *Chylek and Ramaswamy*, 1984].

We now present the different simulations performed to test the impact on the retrieved aerosol optical depth of the aerosol size distribution, the aerosol composition, and the type (heterogeneous versus homogeneous) of particle mixture. Tests were performed for the background and the smoke plume atmospheres as defined in Tables 3 and 5 and will help in elaboration of ensuing uncertainties.

Tests on particle size distributions: Tests presented in this section were achieved with a single component of the aerosol phase. It must be kept in mind that such simple aerosols are poorly representative of the smoke aerosols. We used aerosol models described in Table 4a.

Figure 5 presents the relationship between aerosol optical depth and visible AVHRR albedo for black carbon and organic carbon models with different size distributions. It may be seen in the top of Figure 5 that the increase of τ_a, due to an increase of the black carbon content, leads to a decrease of visible AVHRR albedo. The intensity of this effect depends on the particulate size. The same effect occurs with organic particles with small volume mean radius. However, tests show that OC particle growth may reverse the phenomenon. Indeed, in the bottom of Figure 5, it may be seen that curve slopes are either negative, when the plume consists of small particles (with a volume mean radius r_v lower than 0.03 μm), or positive, when particles are larger (r_v > 0.03 μm) and the concentrations are high (τ_a > 0.1). This change in the impact of OC particles underlines the need to accurately determine the OC content of smoke aerosols.

The same results are presented in a different way in Figure 6. Now τ_a is fixed at the constant value of 0.5 : AVHRR albedo is then studied as a function of the volume mean radius of particles. Interestingly, an increase of BC volume mean radius from 0.015 μm to 0.8 μm increases the visible AVHRR albedo, showing the predominance of light backscattering versus forward scattering and absorbing. This is in accordance with the increase of single scattering albedo values calculated for each aerosol model, and indicated in Figure 5. For larger particles, this effect is less important. The same effect is observed for organic carbon particles: for a given aerosol optical depth of 0.5, AVHRR albedo varies from 5 to 14%, and a maximum effect on AVHRR albedo

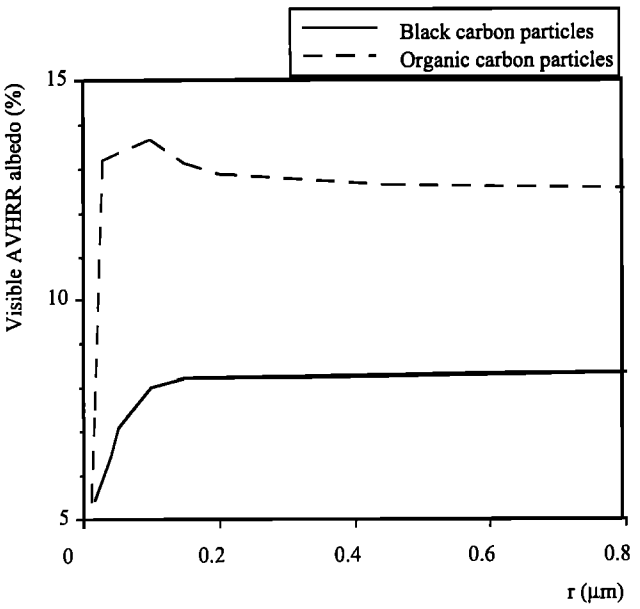

Figure 6. Impact of the volume mean radius on visible AVHRR albedo in % for a constant aerosol optical depth of 0.5. Tests for black carbon and organic carbon particles are plotted separately.

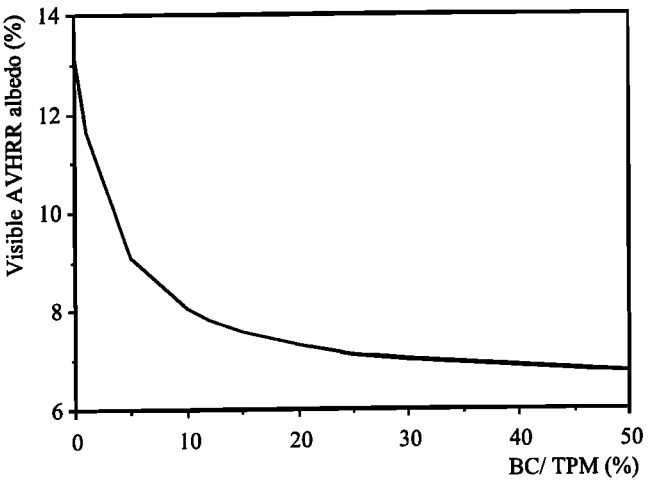

Figure 7. Impact of BC/total particulate matter (TPM) change on the visible AVHRR albedo in % for a constant aerosol optical depth of 0.5 (ratio range observed in biomass burning aerosols : 3-30%). Test for type 1 plume.

is obtained with organic carbon particles with volume mean radius of 0.1 μm and a single scattering albedo of 0.95. Increase of particles over 0.1 μm brings a decrease of visible AVHRR albedo. It may be seen that Figure 6 is in agreement with the theoretical curves of *Twomey* [1977].

Finally, it is possible to use Figure 5 to obtain uncertainties on AVHRR albedo or optical depth due to variation in particle size. Size range is hypothesized to be 0.04-0.8 and 0.03-0.1 μm for BC and OC particles found in both types of plumes. For a given mean AVHRR albedo, it is possible to estimate the effect of particle size on τ_a values. Conversely, for a given aerosol particle depth (τ_a) it is possible to retrieve the size effect on AVHRR albedos. For example, this effect is found to be 25% for BC and 15% for OC models, either for both background or smoke plume conditions. The same investigations were performed for WS and D particles. For the background atmosphere, uncertainties obtained with the use of WS(0.18) or WS(0.8), and that of D(12.2) or D(18) (Table 4a), were found to be of the order of 15-20%.

Impact of the chemical composition of the aerosol mix: Owing to the exceptional absorbing properties of black carbon and its abundance variability in combustion aerosols, a detailed study was designed for the impact of this aerosol component. The visible AVHRR albedo was then calculated as a function of the abundance of black carbon in the carbonaceous aerosol of a type 1 plume for a constant optical depth of 0.5. WS and D particles were fixed as described in Table 5a. Figure 7 shows that the AVHRR signal is greatly affected by the variability of the black carbon abundance. The importance of BC abundance has been previously pointed out by *Bergström et al.* [1982] when calculating particulate optical properties. We show here that its abundance in the atmospheric column is also important. It may be stressed that AVHRR albedo values display the most important variability for the range of BC/TPM values experimentally measured (3-30%). A 50% error in the BC content in the aerosol phase yields an uncertainty of 12% for visible AVHRR albedo. Using Figure 4, this leads to an uncertainty on τ_a of the order of 30%. The same quantitative results have been obtained for type 2 plumes.

With the relationship between BC/TPM and visible AVHRR albedo shown in Figure 7, it is possible to retrieve from satellite data, BC/TPM values in smoke. The mean AVHRR albedo value measured in type 1 plumes over western Africa is of the order of 8%, which yields a BC/TPM value of the order of 10%. This is in agreement with ground-based measurements of smoke plumes [*Cachier et al.*, 1995].

The same kinds of tests have been realized to study the impact of OC, dust, and WS on the visible AVHRR signal. The total uncertainty for τ_a assessed from a given A%, assuming an error of ±50% in the relative concentrations of these components, is of the order of 30%.

Impact of the presence of internally mixed particles: Table 6 presents, for a constant aerosol optical depth of 0.5, the impact on visible AVHRR albedo values, of shells of organic carbon, water-soluble particles or water onto BC particles. The aerosol models are described in Table 4b. In each simulation, the whole aerosol phase was considered to be internally mixed.

Results in Table 6 show that the presence of a thin coating increases the BC particle absorptive capacity (radius being

Table 6. Impact of Different Coatings on Black Carbon Particles, on the Visible AVHRR Albedo (τ_a=0.5)

Aerosol Model	Visible AVHRR Albedo, %
$BC^{(08)}$ (reference)	8.34
BC/OC1%	8.33
BC/OC10%	8.29
BC/water1%	8.50
BC/water10%	8.31
BC/WS1%	8.32
BC/WS10%	8.27

The index gives the nature of the coating (organic carbon, water or WS) and the contribution of the coating to the total volume of particles (1 or 10%).

Table 7. Sensitivity Tests and Overall Absolute Uncertainty on the Aerosol Optical Depths τ_a and Visible AVHRR Albedo A Retrieval

Source of Errors	Errors on τ_a, %	Error on A, %	Text Section
AVHRR albedo	50	8	3.3.3
Viewing geometry	10	3.1	3.3.1
Surface albedo	10	3.1	3.3.1
Gaseous composition	10	3.1	3.3.1
Aerosol model			
Particle size distribution			3.3.2
Water soluble	0	0	
Dust.like	0	0	
Black carbon	25	8.5	
Organic carbon	15	4	
Aerosol composition			3.3.2
Cb/TPM concentration	30	9.6	
Other than black carbon	30	9.6	
Type of mixture (internal/external)	5[a]	1.8[a]	3.3.2
Overall error, %	73	20	

[a]Type 2 plumes only.

constant): single scattering albedo values are decreased from 0.5 to 0.495, which consequently produces a decrease in AVHRR albedo. Within the coating size range considered here (1 to 10% in volume), the increase of coating material at constant size has a more significant impact.

The same tests have been realized for particles having a core of dust coated by organic or sulfate particles. A similar but more important impact than for soot particles is found. This could be explained by the coarser size of dust particles, which enhances the coating effects [*Fenn and Oser*, 1965]. The impact of a water shell on organic carbon particles was also checked. No significant effect on the visible AVHRR albedo could be found. This may be explained by the nature of the organic carbon core, which is less absorbing than black carbon particles and smaller in size than dust particles.

From these tests, the relative error introduced by the choice of either homogeneous particles or heterogeneous particles is calculated to be of the order of ±5%. However, this work deserves further investigations for particles with different core and shell sizes. Focus should be also put on heterogeneous particles deeply mixed in volume, which are a more satisfactory imitation of real aerosol and are thought to have exceptional optical properties [*Ackerman and Toon*, 1981; *Chylek et al.*, 1995; *Haywood and Shine*, 1995].

3. 3. 3. Overall uncertainty on the retrieved aerosol optical depth. Table 7 summarizes the different absolute uncertainties relative to the different parameters used in the retrieval of τ_a. Uncertainty due to AVHRR albedo determinations (50%) was obtained experimentally from errors on AVHRR images as described in section 2.2 (of the order of 8%) and the relationship between visible AVHRR albedo and τ_a (Figure 4). The larger uncertainties are primarily due to the aerosol composition and size distribution. The overall uncertainty on τ_a values retrieved from satellite images is roughly estimated as the quadratic average of the different uncertainties and is found to be of the order of ±75% within the background and the plumes.

Conversely, it is also interesting to investigate how the major model parameters and assumptions affect the observed satellite signal. For this purpose, a simple way is to use the relationship between visible AVHRR albedo and τ_a (Figure 4). Errors on AVHRR albedo retrieval for a constant 0.5 aerosol optical depth are then determined from uncertainties on τ_a retrieval displayed in Table 7. It may be seen that this set of errors is sytematically lower by a factor of 3 than that established for τ_a.

4. Yearly Aerosol Flux Estimates From African Savanna Fires

In spite of the large uncertainty found on τ_a retrieved from AVHRR images, it is interesting and tempting to derive plume aerosol mass from these results. Such a work needs calculations of specific extinction cross section and estimates of global burnt areas. Each of these parameters would deserve a dedicated study. The purpose of this paragraph is then to see if AVHRR results reasonably compare with other measurements.

4. 1. Calculation of Specific Extinction Cross Sections

It is generally accepted that the extinction coefficient (b_e in m^{-1}) at an altitude z is proportional to the aerosol mass concentration (TPM) through the specific extinction cross section σ [*Van de Hulst*, 1957; *Japar et al.*, 1984]:

$$b_e = \sigma \, \mathrm{TPM} \tag{3}$$

The aerosol optical depth is an integration over a vertical atmospheric column and can be expressed as a function of σ and of the aerosol mass (TPM_z) integrated in the vertical column in which the aerosol type is supposed homogeneous :

$$\tau_a = \int_z \sigma \, \mathrm{TPM} \, dz = \sigma \, \mathrm{TPM}_z \tag{4}$$

Thus σ is a critical coefficient for deriving suspended aerosol mass from aerosol optical thickness. As shown in Table 8a, σ

Table 8. Smoke Specific Extinction Cross Sections at 550 nm Reported in the Literature and Calculated for the Aerosol Models Defined in Table 5a

	σ, $m^2 g^{-1}$	Reference
Smoke aerosol		
	3 57	*Tangren* [1982]
	3.73	*Ferrare et al.* [1990]
	3.73	*MacMahon* [1983]
> 0.15 μm	3.57	*Pueschel et al.* [1988]
> 0.3 μm	4.54	*Radke et al.* [1988]
Dry smoke	4.5	*Radke et al.* [1988]
Smoke aerosol with 50% of water	9	*Tangren*[1982]
Dry smoke	4.5	*Liousse et al.* [1994, 1996]
Wet smoke	7	*Liousse et al* [1994, 1996]
Smoke from SCAR-C	5	*Martins et al.* [1997]

Aerosol models	σ, at 550 nm, $m^2 g^{-1}$	
$OC^{(0\,03)}$	0.47	
$OC^{(0\,1)}$	2.505	
$BC^{(0\,04)}$	7	
$BC^{(0\,8)}$	2.01	
$D^{(1\,2\,2)}$	0.101	
$D^{(1\,8)}$	0.1	
$WS^{(0.18)}$	2.6	
$WS^{(0\,8)}$	2	
$BC^{(0\,8)}$/OC	2	
$BC^{(0\,8)}$/water	2	
$D^{(1\,2\,2)}$/OC	0.1	
$D^{(1\,2\,2)}$/water	0.1	
$WS^{(0\,8)}$/OC	2	
$WS^{(0\,8)}$/water	2	
Type 1 Plumes	1.3[a]	1.7[b]
Type 2 Plumes	2 4[a]	4.6[b]
Background	1 [a]	1.35[b]

For internally mixed aerosols, coatings represent 10% of particle volumes.
[a]Calculated from weighted contributions of each type of aerosol model.
[b]Calculated from weighted contributions of each type of aerosol model, assuming a coating of 50% of water surrounding organic carbon and water-soluble particles.

values found in the literature data for smoke aerosols are included in a large range of values (3.5-9 $m^2 g^{-1}$). This may be due to differences in experimental protocols but is primarily linked to the actual variability of smoke aerosol [*Liousse et al.*, 1993].

The σ determination is thus very difficult to obtain because of the conjunctions of several factors. The value of σ varies with particle size, which itself is variable in space and time, but also with particulate density and shape. Also, σ depends on particle chemical composition and the type of aerosol mixture (internal versus external mixture). The impact of water coating is particularly difficult to assess owing to the temporal variability of relative humidity but also its spatial variability, especially with altitude.

Using Mie theory [*Van de Hulst*, 1957], we computed σ values for the aerosol models chosen for the three typical situations described above. The σ values obtained are displayed in Table 8b. They are found to be slightly affected by the presence of coatings. The trend is then an increase of absorption coefficients, and a decrease of scattering coefficients.

For the background atmosphere and the two plume models, σ values were calculated by summing weighted contributions of each aerosol type. Specific extinction cross sections were calculated to be 1, 1.3, 2.4 $m^2 g^{-1}$. These values are lower than those described in the literature (Table 8a). In light of recent results and among different parameters, the importance of water coating could be significant. *Kaufman et al.* [1990a,b, 1994] found that, in forest fires, at 70% relative humidity at least half of the total particle mass could be constituted by water. We recall that, following previous works, in our study the water shell represents only 1 to 10% of the particulate volume. *Kiehl and Briegleb* [1993] have shown that for sulfate particles with 50% water volume, σ was multiplied by a factor of 2. If such a hypothesis may also apply to OC particles, σ values for smoke would be 1.35, 1.7, and 4.6 $m^2 g^{-1}$ for the background atmosphere, type 1 and type 2 plumes, respectively. It appears that change in σ values is significant for type 2 plumes only. In order to use extinction cross section values adapted to more realistic situations, we decided to adopt this set of values for further calculations.

A large uncertainty (over 100%) is generated by the choice of

the different aerosol models (Table 8). Furthermore, it must be kept in mind that this uncertainty could be still more significant if variations in chemical composition and type of mixtures were included.

4. 2. Estimate of the Aerosol Mass in Plumes

Using specific extinction coefficients previously calculated (Table 8b) and the aerosol optical depths presented in Table 2, the aerosol concentrations in plumes and background atmosphere have been calculated. Results are given in Table 2. The average total aerosol load in the background atmosphere is about 0.07 g m^{-2}. In the mean type 1 plume, it is estimated to be 0.195 g m^{-2} (or 0.265 if the background contribution is included), and 0.04 in the mean type 2 plume (or 0.11 g m^{-2} if the background is included). Considering that both types of plume structures have approximatively the same average size (100 km^2), the average plume type 1 and type 2 aerosol mass loadings are 19.5×10^6 g and 4×10^6 g, respectively. These values are given with a factor of 5 uncertainty, which is roughly calculated as the quadratic average of the different uncertainties linked to average plume size determinations (which may be assumed to be of the order of 2) and to τ_a and σ determinations which have been described above.

4. 3. Estimate of the Aerosol Flux from African Savanna Fires

Having estimated average aerosol mass loadings in both smoke plume types, our purpose is now to evaluate the total aerosol mass emitted by the whole savanna burning source in Africa. Since all the plume events could not be detected from the images, a simple flux calculation performed from the determination of smoke plume extent and number was impossible. The total yearly flux (F) was then estimated as:

$$F = M S_b / s \quad (5)$$

where M, in g/m^2, is the total average aerosol loading taking into account both kinds of smoke plumes; S_b is the yearly burning scarred areas of African savannas, estimated of the order of 6×10^{12} m^2 by *Menaut et al.* [1991] and *Delmas et al.* [1991] from AVHRR data, given with a factor of 2 or 3 uncertainty [*Lacaux et al.*, 1993, 1995]; and s is the mean burned area per smoke plume, estimated in two different ways. First, s may be determined from the evaluation of the burned area per active fire:

$$s = l\, v\, t \quad (6)$$

where l is the mean fire width (about 500 m [*Vickos*, 1991]), v the fire spreading rate assimilated to the mean surface wind speed, and t the time duration of the fire. Here v and t are 1 m/s and 10 hours, respectively, according to the observation of the day-night fire pattern [*Liousse and Cachier*, 1992]). Parameter s is then of the order of 18 km^2. Considering that mean smoke plume area is 100 km^2, s represents 18% of this area.

Second, in each smoke plume structure, the small part where AVHRR albedo values are systematically minimum may be considered as the burned area of the smoke plume. In our plume studies, this area is of the order of 10 km^2; s should then assumed to be about 10%.

With a mean s value of 14% (which is the average of the two previous estimations) and recalling that 90% of the plumes are type 1 and 10% type 2, the total aerosol flux emitted by the African savanna fires is then 7.7×10^{12} g. Considering that in this region, 85% of the total particulate matter is composed of carbonaceous aerosols [*Cachier et al.*, 1995], total carbon flux may be estimated to be of 6.5×10^{12} gC. As the Cb/TPM value is of the order of 10% in plumes, the flux of black carbon is about 1×10^{12} g. Taking into account high uncertainties, especially linked to the burnt area estimates, it may be assessed that these values are obtained with a factor of 5 uncertainty.

In spite of these large uncertainties, the remote-sensing-derived flux evaluation (6.5 TgC/yr) compares with the value estimated from the ground-based measurements of carbonaceous particles (13 TgC/yr [*Cachier et al.*, 1995]). These values are lower than those found by *Radke et al* [1989]. The difference is primarily due to the larger particle emission factor used by these authors, and derived from forest fire experiments. Indeed, forest fires cause twice as high particulate emissions due to the importance of the smoldering phase, whereas savannas primarily burn under «cleaner» flaming conditions.

5. Conclusions

For the first time to our knowledge, this work shows that the detection of savanna smoke plumes on AVHRR images is possible and may further lead to aerosol loading estimates. Owing to the savanna albedo values which are included in the range of critical surface albedo values, the spatial detection of smoke structures is difficult and sometimes impossible. Over a given region, the effect of smoke may produce either an increase (type 2 plumes) or a decrease (type 1 plumes) of visible AVHRR albedo, depending on the aerosol properties.

We suggest that optical impact of smoke depends primarily on the combustion nature and intensity which affects the vertical buoyancy of the smoke plume, the concentrations, and the physical and chemical properties of the aerosols. Thus the type 2 plume structures could result from a more intense combustion than the type 1 plumes with a higher vertical development. In such a case, particles are expected to gain rapidly the habit of old aerosols : as shown by sunphotometer data, their size is centered in the accumulation mode. They are also mostly internally mixed. Moreover, fires which produce such plumes are incomplete combustions and have been shown to produce relatively more organic carbon particles than less intense fires. All these phenomena consequently favor the increase of single scattering albedo of the type 2 plumes.

The 5S radiative transfer model was adapted to remote sensing of savanna biomass burning aerosols. New smoke aerosol models based on chemical and optical properties measured in the field were included; the heterogeneous nature of the particles has been also considered. Aerosol optical depths of about a hundred smoke plumes were retrieved, and carbonaceous aerosol mass assessed. Aerosol optical depth at 550 nm was found to be of the order of 0.5 in smoke plumes and 0.1 in the background atmosphere. Aerosol optical thickness determinations were shown to be highly dependent on the smoke aerosol size distribution and composition, especially on BC abundances in the aerosol mix. On the contrary, the nature of aerosols is not an essential parameter, since the extinction coefficient is similar for a two-component internal mixtures (with a volume ratio up to 10%) or external mixtures as long as the size distribution are identical in both computations. A careful study of the water impact is needed, since relative humidity has been seen to highly influence the optical properties of aerosols [*Pilinis et al.*, 1995]. Effort has also to be put in experimental measurements of particle refractive index, density, and asymmetry factor. An improvement would

finally reside in the consideration of aerosol volume mixtures and nonspherical particles.

Specific extinction cross sections (ratio between the aerosol optical depth and the aerosol vertically integrated mass loading) were estimated to obtain the total aerosol mass in an average smoke plume of each type. Values obtained are of the order of 19.5×10^6 g and $4.\times 10^6$ g for type 1 and type 2 plumes, respectively. We estimated a total mass of carbonaceous particles emitted by African biomass burning of 6.5 TgC per year with a factor of 5 of uncertainty. This result is in the same order of magnitude as estimations based on ground measurements (13 TgC per year).

Acknowledgments. This work is part of the DECAFE programme funded by CNRS and Ministère de l'Environnement in France. Some computing facilities were kindly provided by the Laboratoire de Modélisation du Climat et de l'Evironnement (LMCE), Commissariat à l'Energie Atomique. We wish to thank J.-P. Malingreau and J.-M. Grégoire from the EEC Joint Research Centre at Ispra for providing images. Helpful discussions with J.-M. Brustet and collaboration with R Franca (Laboratoire d'Aérologie) for fire mapping are gratefully acknowledged. We also thank F. Guillard, C. Moulin, and J. Poitou (LMCE) for helpful computing and scientific assistance, and J.-C. Menaut (Laboratoire d'Ecologie) and J.-P. Lacaux (Centre de Recherches Atmosphériques) for useful scientific assistance and comments. This is a CFR contribution n°1928.

References

Ackerman, T.P., and O.B Toon, Absorption of visible radiation in atmosphere containing mixtures of absorbing and nonabsorbing particles, *Appl. Opt., 20*, 3661-3667, 1981.

Andreae, M.O., E.V. Browell, M Garstang, G.L Gregory, R.C. Harriss, G.F. Hill, D.J. Jacob, M.C. Pereira, G.W. Sachse, A.W. Setzer, P.L. Silva Dias, R.W. Talbot, A.L. Torres, and S.C. Wofsy, Biomass-burning emissions and associated haze layers over Amazonia, *J. Geophys. Res.* 93, 1509-1527, 1988.

Andreae, M.O., Biomass burning· Its history, use and distribution and its impact on environmental quality and global climate, in *Global Biomass Burning*, edited by J. S. Levine, pg. 1-21, MIT Press, Cambridge, Mass., 1991.

Andreae, M.O., B.E. Anderson, D.R. Blacke, J.D. Bradshaw, J.E. Collins, G.L. Gregory, G.W. Sachse, and M.C. Shipham, Influence of plumes from biomass burning on atmospheric chemistry over the equatorial and tropical South Atlantic during CITE 3, *J. Geophys. Res., 99*, 12,793-12,808, 1994.

Arino, O., G. Dedieu, and P Y. Deschamps, Determination of land surface spectral reflectances using Meteosat and NOAA/AVHRR shortwave channel data, *Int J. Remote Sens., 13*, 2263-2287, 1992.

Bergström, R.W., Predictions of the spectral absorption and extinction coefficients of an urban air pollution aerosol model, *Atmos. Environ., 6*, 247-258, 1972.

Bergström, R.W., T.P. Ackerman, and L.W. Richards, The optical properties of particulate elemental carbon, in *Particulate Carbon: Atmospheric Life Cycle*, edited by G.T. Wolff and R.L. Klimisch, pg. 43-49, Plenum Press, New York-London, 1982.

Bony, J.P., Bilan radiatif du rayonnement solaire au dessus d'une savane moyenne de Cote d'Ivoire (Lamto), Ph.D. thesis, 148 pp., Univ. Paris Sud, 1975.

Brustet, J.M., J. Vickos, J. Fontan, K. Manissadjan, A. Podaire, and F. Lavenu, Remote sensing of biomass burning in West Africa with NOAA-AVHRR, in *Global Biomass Burning*, edited by J. S. Levine, pp. 47-52, MIT Press, Cambridge, Mass., 1991.

Cachier, H., Combustion carbonaceous aerosols in the atmosphere. Implications for ice-core studies, in *Ice Core Studies of Biogeochemical Cycles, NATO ASI Ser.*, Vol. (1) 30, edited by R. Delmas, pp. 347-360, Springer-Verlag, New York, 1995.

Cachier, H., J. Ducret, M.P. Brémond, V. Yoboué, J.P. Lacaux, A. Gaudichet, and J. Baudet, Biomass burning aerosols in a savanna region of the Ivory Coast, in *Global Biomass Burning*, edited by J. S. Levine, pp. 174-180, MIT Press, Cambridge, Mass., 1991.

Cachier, H., C. Liousse, P. Buat-Ménard, and A. Gaudichet, Particulate content of savanna fire emissions, *J. Atmos. Chem., 22*, 123-148, 1995.

Che, N., and J.C. Price, Survey of radiometric calibration results and methods for visible and near infra-red channels of NOAA-7,9, and -11 AVHRRs, *Remote. Sens. Environ., 41*, 19-27, 1992.

Chung, Y.S., and H.V. Le, Detection of forest-fire smoke plumes by satellite imagery, *Atmos. Environ., 18*, 2143-2151, 1984.

Chylek, P , V. Ramaswamy, R. Cheng, and R G Pinnick, Optical properties and mass concentration of carbonaceous smokes, *Appl. Opt* 20, 2980-2984, 1981

Chylek, P., and V. Ramaswamy, Effect of graphitic carbon on the albedo of clouds, *J. Atmos. Sci., 41*, 3076-3084, 1984.

Chylek, P., G. Videen, D. Ngo, and R.G. Pinnick, Effect of black carbon on the optical properties of sulfate aerosols, *J Geophys. Res., 100*, 16,325-16,332, 1995.

D'Almeida, G.A., P. Koepke, and E.P Shettle, *Atmospheric Aerosols: Global Climatology and Radiative Characteristics*, 561 pp., A. Deepak, Hampton, Va., 1991.

Delmas, R., P. Loudjani, and A. Podaire, Biomass burning in Africa: An assessment of annually burnt biomass, in *Global Biomass Burning*, edited by J.S. Levine, pp 126-132, MIT Press, Cambridge, Mass., 1991.

Dulac, F., D. Tanré, G. Bergametti, P. Buat-Ménard, M. Desbois, and D. Sutton, Assessment of the African dust mass over the western Mediterranean Sea using Meteosat data, *J. Geophys. Res., 97*, 2489-2506, 1992.

Echalar, F.A., Caractérisation de la fraction minérale des particules émises par les feux de végétation tropicale, Ph.D. thesis, 287 pp , Univ. Paris XII, France, 1995.

Fenn, R.W., and H. Oser, Scattering properties of concentric soot-water spheres for visible and infra-red light, *Appl. Opt , 4*, 1504-1509, 1965.

Ferrare, R., R.S. Fraser, and Y.J. Kaufman, Satellite measurements of large-scale air pollution: Measurements of forest fire smoke, *J. Geophys. Res. , 95*, 9911-9925, 1990.

Fishman, J., C.E. Watson, J.C. Larsen, and J.A. Logan, Distribution of tropospheric ozone determined by satellite data, *J. Geophys. Res., 95*, 3599-3617, 1990.

Franca, J.R.A., J.M. Brustet, and J. Fontan, Multispectral remote sensing of biomass burniing in West Africa, *J. Atmos. Chem., 22*, 81-110, 1995.

Fraser, R.S., and Y.J. Kaufman, The relative importance of scattering versus absorption in remote sensing, *IEEE Trans. Geosci. Remote Sens., 23*, 625-633, 1985.

Fraser, R.S., Y.J. Kaufman, and R.L. Mahoneh, Satellite measurements of aerosol mass and transport, *Atmos. Environ., 18*, 2577-2584, 1984.

Grégoire, J.M., A.S. Belward, and P. Kennedy, Dynamiques de saturation du signal dans la bande 3 du senseur AVHRR: Handicap majeur ou source d'information pour la surveillance de l'environnement en milieu soudano-guinéen d'Afrique de l'Ouest, *Int. J. Remote Sens., 14*, 2079-2095, 1993.

Gutman, G., A. Gruber, D. Tarpley, and R. Taylor, Application of angular models to AVHRR data for determination of the clear-sky planetary albedo over land surfaces, *J. Geophys. Res., 94*, 9959-9970, 1989.

Haywood, J.M., and K.P. Shine, The effect of anthropogenic sulfate and soot aerosol on the clear sky planetary radiation budget, *Geophys. Res. Lett., 22*, 603-606, 1995.

Herring, J A., R.J. Ferek, and P.V. Hobbs, Heterogeneous chemistry in the smoke plume from the 1991 Kuwait oil fires, Paper presented at the conference on *Biomass Burning and Global Change*, NASA Langley Research Center, Williamsburg, Va., March 1995.

Hobbs, P.V., J.S. Reid, J.A. Herring, J.D. Nance, R.E. Weiss, J.L. Ross, D.A. Hegg, R.D. Ottmar, and C. Liousse, Particle and trace gas measurements in the smoke from prescribed burn of forest products in the Pacific Northwest, in *Biomass Burning and Global Change*, edited by J.S. Levine, MIT Press, Cambridge, Mass., in press, 1997.

Holben, B.N., Y.J. Kaufman, and J.D. Kendall, NOAA-11 AVHRR visible and near infra-red inflight calibration, *Int. J. Remote Sens., 11*, 1511-1519, 1990.

Holben, B. N , Y.J. Kaufman, A.W. Setzer, D. Tanré, and D.E. Ward, Optical properties of aerosol emissions from biomass burning in the tropics, BASE-A, in *Global Biomass Burning*, edited by J. S. Levine, pp. 403-411, MIT Press, Cambridge, Mass., 1991.

Japar, S.M., A.C. Szkarlat, and W.R. Pierson, The determination of the

optical properties of airborne particle emissions from diesel vehicles, *Sci. Total Environ.*, *36*, 121-130, 1984.

Kaufman, Y.J., Satellite sensing of aerosol absorption, *J. Geophys Res.*, *92*, 4307-4317, 1987.

Kaufman, Y J., and B.N. Holben, Calibration of the AVHRR visible and near-IR bands by atmospheric scattering, ocean glint and desert reflection, *Int. J. Remote Sens.*,*14*, 21-52, 1993.

Kaufman, Y.J., C.J. Tucker, and I. Fung, Remote sensing of biomass burning in the tropics, *J.Geophys.Res.*, *95*, 9927-9939, 1990a.

Kaufman, Y.J., R.S. Fraser, and R.A. Ferrare, Satellite measurements of large-scale air pollution: Methods, *J. Geophys. Res.*, *95*, 9895-9909, 1990b.

Kaufman, T.J., A. Setzer, D. Ward, D. Tanré, B N. Holben, P. Menzel, M.C. Pereira, and R. Ramussen, Biomass burning airborne and spaceborne experiment in the Amazonas (Base A), *J. Geophys. Res.*, *97*, 14,581-14,599, 1992.

Kaufman, Y.J., B.N. Holben, D. Tanré, and D.E. Ward, Remote sensing of biomass burning in the Amazon, *Remote Sens. Rev.*, *10*, 51-90, 1994.

Kiehl, J.T., and B.P. Briegleb, The relative roles of sulfate aerosols and greenhouse gases in climate forcing, *Science*, *260*, 311-314, 1993.

King, M.D., Y.J. Kaufman, W.P. Menzel, and D. Tanré, Remote sensing of cloud, aerosol, and water vapor properties from the moderate resolution imaging spectrometer (MODIS), *IEEE Trans. Geosci. Remote Sens.*, *30*, 2-27, 1992.

Lacaux, J.P., H. Cachier, and R. Delmas, Biomass burning in Africa: An overview of the impact on the atmospheric chemistry, in *Fire in the Environment: Ecological, Climatic and Atmospheric Chemical Importance*, edited by P.J. Crutzen and J.G. Goldammer, pp. 159-191, John Wiley, New York, 1993.

Lacaux, J.P., J.M. Brustet, R. Delmas, J.C. Menaut, L. Abbadie , B. Bonsang, H Cachier, J.G.R. Baudet, M.O. Andreae, and G. Helas, Biomass burning in the tropical savannas of Ivory Coast: An overview of the field experiment fire of Savanna (FOS-DECAFE 91), *J. Atmos. Chem.*, *22*, 195-216, 1995.

Le Canut, P., M.O. Andreae, G.W. Harris, F.G. Wienhold, and T. Zenker, Airborne studies of emissions from savanna fires in southern Africa, I., Aerosol emissions measured with a laser optical particle counter, *J. of Geophys Res.*, *101* (D19), 23,615-23,630, 1996.

Levine, J.S., Global biomass burning: Atmospheric, climatic and biospheric implications, *EOS Trans. AGU*, *71* (37), 1075-1077, 1990.

Lijlas, E., Automated recognition of cloud types from satellites and its application to nowcasting, in *International Conference on Agrometeorol.*, pp. 27-46, Fondazione Cesena Agric., Cesena, Italy, 1987.

Liousse, C., and H Cachier, Measurement of black carbon aerosols in the atmosphere of two different regions: Real time data for the Paris region and a Savannah site of the Ivory Coast, *Environ. Tech. Lett.*, *13*, 959-967, 1992.

Liousse, C., H. Cachier, and S.J. Jennings, Optical and thermal measurements of black carbon aerosol content in different environments: Variation of the specific attenuation cross-section, sigma (s), *Atmos. Environ.*, *27A*, 1203-1211, 1993.

Liousse, C , H. Cachier, F. Dulac, D. Tanré, C. Devaux, S.G. Jennings, A. Gaudichet, P. Echalar, and J.E. Penner, Biomass burning aerosols: Improved optical properties and revised global radiative impact (abstract), in *Fourth International Aerosol Conference, Los Angeles*, p. 855, American Association for Aerosol Research, Cincinnati, OH, USA, 1994.

Liousse, C., C. Devaux, F. Dulac, and H. Cachier, Aging of savanna biomass burning aerosols. Consequences on their optical properties, *J. Atmos. Chem* , *22*, 1-17, 1995.

Liousse, C., J.E. Penner, C. Chuang, J.J. Walton, H. Eddleman, and H. Cachier, A global three-dimensional model study of carbonaceous aerosols, *J Geophys. Res. 101*(D4), 19,411-19,432, 1996.

MacMahon, C.K., Characteristics of forest fuels, fires and emissions, paper presented at 76th Annual Meeting, Air Pollut. Assoc., Atlanta, Ga., 1983

Malingreau, J.P., The contribution of remote sensing to the global monitoring of fires in tropical and subtropical ecosystems, in *Fire in the Tropical Biota*, edited by J.C. Goldammer, pp. 337-368, John Wiley, New York, USA, 1990.

Malingreau, J.P., C.J. Tucker, and N. Laporte, AVHRR for monitoring global tropical deforestation, *Int. J. Remote Sens.*, *10*, 855-867, 1989.

Martins, J.V., P. Artaxo, C. Liousse, H. Cachier, Y. Kaufman, and A.P. Fattori, Size distribution, elemental composition, carbon measurements, and calculated optical properties of biomass burning aerosol particles during the SCAR-C experiment, in *Biomass Burning and Global Change*, edited by J.S. Levine, MIT Press, Cambridge, Mass., in press, 1997.

Mazurek, M.A., W.R Cofer, and J.S. Levine, Carbonaceous aerosols from prescribed burning of a boreal forest ecosystem, in *Global Biomass Burning*, edited by J. S. Levine, 258-263, MIT Press, Cambridge, Mass , 1991.

McClatchey, R.A., R.W. Fenn, J.E A. Selby, F.E. Voltz, and J.S. Garing, Optical properties of the atmosphere, *Rep. AFCRL-TR-71-0279, Environ. Res Pap 354*, Air Force Cambridge Res Lab., Bedford, Mass, 1971

McCormick, M.P., and R.E. Veiga, SAGE II measurements of early Pinatubo aerosols, *Geophys. Res. Lett., 19*, 155-158, 1992.

Menaut, J C , L. Abbadie, F. Lavenu, P Loudjani, and A. Podaire, Biomass burning in west African savannas, in *Global Biomass Burning*, edited by J. S. Levine, pp. 133-142, MIT Press, Cambridge, Mass., 1991.

Monnier, Y., Les effets des feux de brousse sur une savane préforestière de Côte d'Ivoire, *Etudes Eburnéennes, 9*, 260 pp., 1968.

Parungo, F., B. Kopcewicz, C. Nagamoto, R. Schnell, P Sheridan, C. Zhu, and J. Harris, Aerosol particle in the Kuwait oil fire plumes: Their morphology, size distribution, chemical composition, transport and potential effect on climate, *J. Geophys. Res., 97*, 15,867-15,882, 1992.

Patterson, E.M., and D.A. Gillette, Commonalities in measured size distributions for aerosols having a soil-derived component, *J. Geophys. Res.*, *82*, 2074-2082, 1977.

Penner, J.E., S.J. Ghan, and J J. Walton, The role of biomass burning in the budget and cycle of carbonaceous soot aerosols and their climate impact, in *Global Biomass Burning*, edited by J. S Levine, pp. 387-393, MIT Press, Cambridge, Mass., 1991.

Penner, J.E., R.E. Dickinson, and C.A. O'Neill, Effects of aerosol from biomass burning on the global radiation budget, *Science*, *256*, 1432-1433, 1992.

Pilinis, C., S.N. Pandis, and J.H. Seinfeld, Sensitivity of direct climate forcing by atmospheric aerosols to aerosol size and composition, *J. Geophys. Res., 100*, 18,739-18,754, 1995

Porter, J.N., and A.D. Clarke, Aerosol size distribution models based on in situ measurements: Aerosol backscatter calculations, *J. Geophys Res.*, in press, 1997.

Pueschel, R.F., J.M. Livingston, P.B. Russel, D.A. Colburn, T.P. Ackerman, D.A. Allen, B.D. Zak, and W. Einfeld, Smoke optical depths: Magnitude, variability, and wavelength dependence, *J. Geophys. Res.*, *93*, 8388-8402, 1988.

Radke, L.F., D.A. Hegg, J.H. Lyons, C.A. Brock, P.V. Hobbs, R. Weiss, and R. Rasmussen, Airborne measurements on smokes from biomass burning, in *Aerosols and Climate*, edited by P. Hobbs and P. McCormick, pp. 411-421, A. Deepak, Hampton, Va., 1988.

Radke, L.F., J.A. Coakley, and M.D. King, Direct and remote sensing observations of the effects of ships on clouds, *Science*, *246*, 1146-1149, 1989.

Richmond, M.M., and R.C. Flagan, Structure evolution in aerosol synthesis (abstract), in *Fourth International Aerosol Conference, Los Angeles*, p. 507, American Association for Aerosol Research, Cincinnati, OH, USA, 1994.

Robock, A., Surface cooling due to forest fire smoke, *J. Geophys. Res.*, *96*, 20,869-20,878, 1991.

Rosen, H., and T. Novakov, Role of graphitic carbon particles in atmospheric radiation and transfer, in *Aerosol and Their Climate Effects*, edited by H.E. Gerber and A. Deepak, pp. 83-94, A. Deepak, Hampton, Va., 1984.

Roujean, J.L., M. Leroy, and P.Y. Deschamps, A bidirectional reflectance model of the Earth's surface for the correction of remote sensing data, *J. Geophys. Res.*, *97*, 20,455-20,468, 1992.

SATMOS, *Note d'Information 8*, Centre de Météorol. Spatiale, Lannion, 1991

Seiler, W., and P.J. Crutzen, Estimates of gross and net fluxes of carbon between the biosphere and the atmosphere from biomass burning, *Clim. Change, 2*, 207-247, 1980.

Setzer, A.W., and M.C. Pereira, Amazonia biomass burning in 1987 and an estimate of their tropospheric emissions, *Ambio, 20*, 19-22, 1991.

Sloane, C.S., Optical properties of aerosols: Comparison of measurements with model calculations, *Atmos. Environ.*, *17*, 409-416, 1983

Sloane, C. S., Optical properties of aerosols of mixed composition, *Atmos. Environ., 18*, 871-878, 1984.

Sutton, D., E. Salméron, and F. Dulac, *Système Félix: Guide d'Utilisation,*

180 pp., Cent. Nat. de la Rech. Sci.- CEA, Cent des Faibles Radioactivités, Gif-Sur-Yvette, France, 1988.

Tangren, C.D., Scattering coefficient and particulate matter concentration in forest fire smoke, *J. Air Pollut. Contr Assoc.*, *32*, 729-732, 1982.

Tanré, D., C Deroo, P. Duhaut, M. Herman, J.J. Morcrette, J Perbos, and P.Y Deschamps, Description of a computer code to simulate the satellite signal in the solar spectrum: The 5S code, *Int. J. Remote Sens.*, *2*, 659-668, 1990.

Tanré, D., B. N. Holben, and Y. J Kaufman, Atmospheric correction algorithm for NOAA-AVHRR products. Theory and application, *IEEE Trans. Geosci. Remote Sens.*, *30*, 231-248, 1992.

Twomey, S., *Atmospheric Aerosols*, 302 pp , Elsevier, New York, 1977.

Van de Hulst, H.C., *Light Scattering by Small Particles*, p.144, John Wiley, New York, 1957.

Vickos, J.B., Télédétection des feux de végétation en Afrique intertropicale et estimation des émissions des constituants ayant un intérêt atmosphérique, Ph.D. thesis, 142 pp., Univ. P. Sabatier, Toulouse, France, 1991.

Vogt, J., Calculation of TOA albedo, NDVI, surface temperature and precipitable water content of the atmosphere from NOAA AVHRR data, *Tech. Note, 1.90.72*, Comm. of the Eur. Commun., Joint Res. Cent , Inst. for Remote Sensing Appli , Ispra, Italie, 1990.

Whitby, K.T., The physical characteristics of sulfur aerosols, *Atmos. Environ.*, *12*, 135-159, 1978.

World Meteorological Organization, A preliminary cloudless standard atmosphere for radiation computation, WCP 112, CAS/Radiation Commission of IAMAP, Boulder, Colo., USA, 1986.

Wu, A., and Q. Zhong, A method for determining the sensor degradation rates of NOAA AVHRR channels 1 and 2, *J. Appl. Meteorol* , *33*, 118-122, 1994.

H. Cachier, F. Dulac, and C. Liousse, Centre des Faibles Radioactivités, CNRS-CEA, Ave de la Terrasse, F-91198 Gif sur Yvette, Cedex, France. (e-mail: Helene.Cachier@cfr.cnrs-gif.fr; dulac@asterix.saclay.cea.fr; Catherine.Liousse@cfr.cnrs-gif.fr.)

D. Tanré, Laboratoire d'Optique Atmosphérique, Centre National de la Recherche Scientifique et Université des Sciences et Techniques de Lille, F- 59655 Villeneuve d'Ascq, France (Didier Tanre@univ-lille1.fr).

(Received April 29, 1994; revised October 11, 1996;
accepted October 16, 1996.)